Journal of Sound and Vibration 329 (2010) 1793–1808

Contents lists available at ScienceDirect

Journal of Sound and Vibration

journal homepage: www.elsevier.com/locate/jsvi

Aeroacoustics of T-junctions—An experimental investigation

Mikael Karlsson [a,*], Mats Åbom [b]

[a] KTH Cicero, The Marcus Wallenberg Laboratory for Sound and Vibration Research, Teknikringen 8, 100 44 Stockholm, Sweden
[b] KTH, Linné Flow Centre, Teknikringen 8, 100 44 Stockholm, Sweden

ARTICLE INFO

Article history:
Received 4 March 2009
Received in revised form
18 November 2009
Accepted 19 November 2009
Handling Editor: R.E. Musafir
Available online 29 December 2009

ABSTRACT

An experimental method for determining the aeroacoustic properties of side branch orifices allowing for any combination of grazing and bias flow is presented. The geometry studied, a T-junction, is treated as an active acoustic three-port. The passive properties, describing the reflection and transmission of an incident acoustic wave, are described by a system matrix while the active properties are described by a source vector. Expressions for the acoustic impedance under various mean flow and acoustic incidence configurations are developed. In addition, methods for identifying regions where the system can generate sound, by studying only the passive properties, are discussed. A self-sustained oscillation is triggered at one of the identified regions by coupling a resonant system to the three-port.

1. Introduction

Side branch orifices are common elements in flow duct applications. The dimensions of the orifices, compared to the main duct dimension, range from small (e.g., perforated plates used in liners and silencers) to large (e.g., in ventilation networks, intake and exhaust systems, and pipelines).

The passive acoustic properties of the orifice are often described by the normalized acoustic impedance, $\overline{Z} = r + i\chi$, where r is the acoustic resistance and χ is the acoustic reactance. The mean flow conditions in the duct influence these properties significantly. Previous studies have mainly discussed the effect of grazing flow [1–8], which is relevant for important applications such as perforated liners and side branch resonators. The general trend observed for grazing flow alone is an increase in the resistance and a decrease in the reactance with mean flow. However, there are applications where bias flow—that is, flow through the orifice—is important. Such applications include cross-flow perforated mufflers, duct junctions, and liners designed for cross flow. The grazing and bias flows often are measured separately but combined in a single empirical model (Elnady [9] gives an example and reviews earlier work). Sun et al. [10] investigated grazing/bias flow interaction effects on perforated plates experimentally. Their results show that there is a difference between the grazing–bias outflow and the grazing–bias inflow cases. However, as those results are applicable only to a few types of perforated plate and for low Strouhal numbers, it is difficult to see a clear trend.

Attempts [11,6] have been made to describe the acoustic impedance of single orifices with analytical models. However, Jing et al. [6] and Peat et al. [12] have shown that the correlation to measured data is generally unsatisfactory. Alternatively, a number of empirical models are available, each tuned to a specific configuration. Unfortunately, as Lee and Ih [7] show, the applicability of one model to other configurations is limited. Therefore a more detailed experimental

* Corresponding author.
E-mail addresses: kmk@kth.se (M. Karlsson), matsabom@kth.se (M. Åbom).

0022-460X/$ - see front matter © 2009 Elsevier Ltd. All rights reserved.
doi:10.1016/j.jsv.2009.11.024

investigation into the interaction between the hydrodynamic and acoustic fields occurring at an orifice, using new approaches, is needed in order to create general models.

Another acoustic property worth investigating is the potential amplification and generation of sound by flow–acoustic interaction when the acoustic field interacts with hydrodynamic instabilities in the shear layer formed over the orifice by grazing mean flow [11]. Depending on the Strouhal number, energy can be transferred either to or from the acoustic field by this interaction, amplifying or attenuating the incoming acoustic disturbance, respectively. Under certain conditions [13,14], the amplification may lead to a self-sustained oscillation. This process, often denoted as a whistle, involves shedding of discrete vortices at the leading edge, with the disturbance growing as it is convected downstream. The vortex disturbance interacts with the acoustic field, adding energy to the acoustic oscillation. As shown by Hofmans [15], in a numerical study of the aeroacoustic properties of a T-Junction, the interaction between the hydrodynamic and acoustic fields is influenced by the incidence of the acoustic field.

This work describes an experimental method for determining the acoustic properties—both active and passive—of a side branch orifice subject to grazing and bias flows (separately or simultaneously). The most common experimental procedure in previous studies is the so-called in situ two-microphone method [16]. This measurement method is appealing since the instrumentation is relatively limited, and it works over a wide frequency range. However, the method is sensitive to near-field effects and, more importantly, does not allow the effects of bias flow to be studied. With an impedance tube setup, as used in a modified form by Dickey and Selamet [5] and in a classic form by Sun et al. [10], bias flow can be studied, but the frequency resolution of the measurements is limited by standing wave phenomena in the test rig. More recently, inverse methods [17–20] have been developed for perforated liners, in which the measured attenuation of a propagating wave over a given length of the specimen, often using the two-microphone wave decomposition technique, is used to determine the impedance parameter of a numerical propagation model.

An alternative experimental method is presented here, where the main flow duct, with the attached side branch, is treated as an active acoustic three-port. This method allows the orifice to be subjected to any combination of grazing and bias flows, and also allows variation of the incidence of the acoustic field. In addition, the method can detect sound generation. The geometry tested is a T-junction where the side branch is of the same diameter as the main duct. Results are presented for both the passive and the active acoustic properties for various flow and acoustic field configurations. Additionally, methods for studying the passive acoustic properties of the system, for identifying critical ranges of self-sustained oscillations, are described. Although a discussion of the results follows, no empirical model for the impedance is proposed, as the aim here is to describe a useful tool for determining the aeroacoustic properties of a system with grazing–bias flow rather than to parameterize them.

2. Theory

2.1. The T-Junction as an active acoustic three-port

Any linear time-invariant N-port may be described by relating N input state variables of choice to N corresponding output variables [21]. Using the scattering matrix form, with a vector representing uncorrelated sources in the system, the active acoustic three-port may be defined as

$$\hat{\mathbf{x}}_+ = \mathbf{S}\hat{\mathbf{x}}_- + \hat{\mathbf{x}}^{s+}, \tag{1}$$

where $\hat{\mathbf{x}}$ is the Fourier transform of the state variable of choice, the $+/-$ directions are defined in Fig. 1, and the superscript "s" denotes source. The elements of the scattering matrix $\mathbf{S}$ represent the reflection and transmission coefficients of the

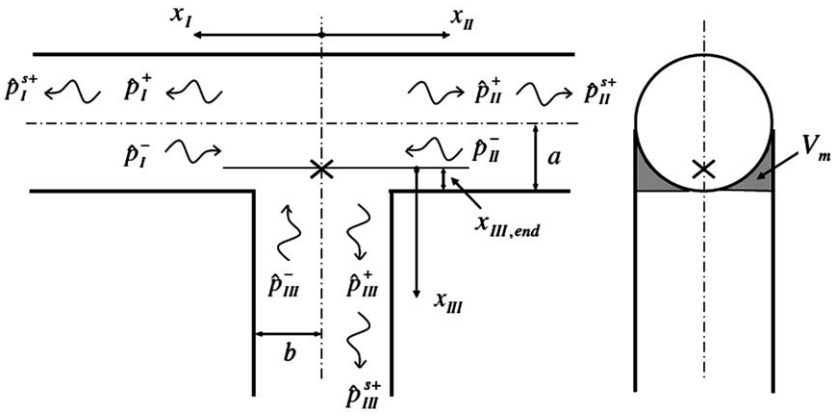

Fig. 1. Definition of coordinate system and acoustic centre (marked with X) for the studied T-junction. The orifice under study is the opening to the side branch (Branch III).

system, R and T, for the given state variable

$$\mathbf{S}=\begin{bmatrix} R_{\mathrm{I}} & T_{\mathrm{II,I}} & T_{\mathrm{III,I}} \\ T_{\mathrm{I,II}} & R_{\mathrm{II}} & T_{\mathrm{III,II}} \\ T_{\mathrm{I,III}} & T_{\mathrm{II,III}} & R_{\mathrm{III}} \end{bmatrix}. \tag{2}$$

Having determined the passive properties, one can proceed to the active part. Rewriting Eq. (1), the source vector is obtained [22]:

$$\hat{\mathbf{x}}^{s+}=(\mathbf{E}-\mathbf{SR})(\mathbf{E}+\mathbf{R})^{-1}\hat{\mathbf{x}}=\mathbf{C}\hat{\mathbf{x}}, \tag{3}$$

where $\mathbf{E}$ is the unit matrix and $\mathbf{R}$ is the reflection matrix characterizing the system terminations (obtained from the passive measurements). An estimate for the source cross-spectrum matrix can now be obtained. However, with direct measurements this matrix involves the autospectra at the reference sections in the three ducts, and autospectra are sensitive to local turbulence at the microphone positions. To improve the result, two reference cross-sections are used to represent each port, with the cross-sections sufficiently separated so that any local turbulence in the measured signals is uncorrelated. The source cross-spectrum estimate then depends only on cross-spectra between fluctuating quantities. The resulting equation is

$$\mathbf{G}^{s}=\mathbf{T}_{+}^{-1}\hat{\mathbf{x}}_{2}^{s+}\hat{\mathbf{x}}_{1}^{s+*}=\mathbf{T}_{+}^{-1}\mathbf{C}_{2}\mathbf{G}^{m}\mathbf{C}_{1}^{*}, \tag{4}$$

where $\mathbf{T}$ is the transformation matrix for the source strength vector between the cross-sections, $\mathbf{G}^{m}$ is a 3×3 matrix containing the measured cross-spectra, * is the Hermitian transpose, and the subscripts 1 and 2 denote the two reference cross-sections. The diagonal elements of the resulting matrix, $\mathbf{G}^{s}$, represent the autospectra of the source quantity at each port. This procedure compensates for resonance effects in the test rig, and the results may be related to the generated noise (outgoing waves with reflection-free terminations) at the three ports.

Eq. (1), which can be extended to the general case of an N-port system, represents a linear aeroacoustic model where the source vector normally is considered independent of the acoustic field [21]. This is often a good assumption when this type of model is applied to various fluid machines [22]. However, in applications with flow-generated sound, vortex–sound interaction effects should be included. One way to do this is to assume that the part of the unsteady flow associated with the acoustic source process can be modulated by the incident acoustic waves. In applying this idea, one postulates that the source strength vector $\hat{\mathbf{x}}^{s+}$, in the general case, can be split into two parts, with one part corresponding to the modulation by an incident acoustic field and the other part independent of the acoustic field. The most general linear time-invariant model for the modulated part is given by $\hat{\mathbf{x}}_{mod}^{s+}=\mathbf{S}_{m}\hat{\mathbf{x}}_{-}$. Inserting this expression into Eq. (1) yields

$$\hat{\mathbf{x}}_{+}=(\mathbf{S}_{0}+\mathbf{S}_{m})\hat{\mathbf{x}}_{-}+\hat{\mathbf{x}}_{0}^{s+}, \tag{5}$$

where the original scattering matrix now is denoted $\mathbf{S}_0$ to emphasize that it represents the part independent of the source coupling, and $\hat{\mathbf{x}}_{0}^{s+}$ is the part of the source strength unmodified by the acoustic field. Hence, a linear modulation of the source term simply adds to the scattering properties. This result implies that in an experimental characterization of an N-port any information on vortex–sound interaction effects is included in the scattering matrix data, while the resulting source vector is always independent of the incident acoustic field.

The interfaces of the three ports are easily transported along the ducts, since plane-wave propagation is assumed. Here the three-port is actually reduced to a single point, marked with a bold X in Fig. 1. It is defined as the point on the axis of the side branch extending a distance $x_{\mathrm{III,end}}$ into the main duct, corresponding to the end correction with zero mean flow. In the case of a circular duct, as used here, this end correction consists of two parts (see, for example, Neederveen et al. [23] or Dubos et al. [24]). One part is the inner end correction, and the other part compensates for the volume V_m resulting from the joining of the ducts (see Fig. 1). The following approximate formulas can be used to calculate the end correction [23]:

$$x_{\mathrm{III,end}}=t_i+t_m, \tag{6}$$

$$t_i=(0.82-1.4\delta^{2}+0.75\delta^{2.7})b, \tag{7}$$

$$t_m=\frac{b\delta}{8}(1+0.207\delta^{3}), \tag{8}$$

where $x_{\mathrm{III,end}}$ is the total end correction shown in Fig. 1, and t_i and t_m are the inner and matching end corrections, respectively. $\delta=b/a$ is the ratio of the inner radii of the side branch and the main duct.

2.2. Aeroacoustic properties of a side branch

A general definition of impedance is the ratio of a potential quantity to a flow quantity, where the product of the two quantities represents power. The usual definition in acoustics is the ratio of the fluctuating pressure to the acoustic volume velocity. However, this definition only complies with the requirement of providing a description of acoustic power in the absence of mean flow. Alternative state variables, with the desired property that their product represent acoustic power in the presence of mean flow [25], are the linearized forms of the fluctuating stagnation enthalpy, h', and mass flow, m', which

yield the impedance Z_h:

$$Z_h = \frac{h'}{m'}, \tag{9}$$

For a homentropic flow $h' = (p'/\rho_0) + U_0 u'$ and $m' = (\rho_0 u' + \rho' U_0)A$, where p is pressure, ρ is density, U_0 is the mean flow velocity, u is the fluctuating velocity, A is the cross-sectional area of the duct, and the prime denotes an acoustic field quantity.

Hence, the most compact choice for the state variable in the definition of the three-port is the fluctuating stagnation enthalpy. However, here the scattering matrix is based on acoustic pressure, as that is the more common choice and the actual entity measured, that is, the fluctuating stagnation enthalpy and mass flow are given in terms of a scattering matrix based on the acoustic pressure. Then, the two variables in Eq. (9) can be rewritten as

$$h' = \frac{p_+}{\rho_0}((1+M)+R(1-M)), \tag{10}$$

$$m' = \frac{p_+ A}{c_0}((1+M)-R(1-M)), \tag{11}$$

where R is the acoustic pressure reflection coefficient. This leads to the following expression for the acoustic impedance in a duct:

$$Z_h = \frac{c_0}{\rho_0 A}\,\frac{(1+M)+R(1-M)}{(1+M)-R(1-M)}. \tag{12}$$

With access to the full scattering matrix for the three-port, we can now study the orifice impedance for an incident wave from any port and with any flow configuration. Assuming anechoic terminations in the two ports where the acoustic wave is not incident, and using the definitions of the three-port in Fig. 1 and the scattering matrix in Eqs. (1) and (2), expressions for the normalized junction impedance, $\overline{Z} = Z_h/(c_0/\rho_0 A_{\mathrm{III}})$, for plane waves incident from Branches I, II, or III, respectively, are as follows:

$$\overline{Z}_{\mathrm{I-III}} = \frac{(1+M_{\mathrm{I}})+R_{\mathrm{I}}(1-M_{\mathrm{I}})}{T_{\mathrm{I-III}}(1 \pm M_{\mathrm{III}})}, \tag{13}$$

$$\overline{Z}_{\mathrm{II-III}} = \frac{(1-M_{\mathrm{II}})+R_{\mathrm{II}}(1+M_{\mathrm{II}})}{T_{\mathrm{II-III}}(1 \pm M_{\mathrm{III}})}, \tag{14}$$

$$\overline{Z}_{\mathrm{III}} = \frac{(1 \pm M_{\mathrm{III}})+R_{\mathrm{III}}(1 \pm M_{\mathrm{III}})}{(1 \pm M_{\mathrm{III}})-R_{\mathrm{III}}(1 \pm M_{\mathrm{III}})}, \tag{15}$$

where the plus and minus signs for the bias Mach number, M_{III}, represents inflow and outflow, respectively, in the Port III case and outflow and inflow in the Port I and Port II cases. The sub index h no longer appears in the expressions, since it is understood that the enthalpy formulation is used unless otherwise stated. Note that if the enthalpy scattering matrix had been used, the expression would not contain the Mach number terms that compensate for the mean flow. They would be included in the enthalpy scattering matrix elements instead.

For comparison, an impedance tube type measurement yields results seen from the side branch, which agrees with the results in Eq. (15), while a two-microphone in situ technique or an inverse method resembles the formulations in Eqs. (13) and (14). One advantage of the proposed test method is that it is not restricted to a specific definition.

At a side branch subjected to grazing flow, the well-known phenomenon of flow–acoustic coupling – which could lead to self-sustained oscillations, or whistling – may occur. Hydrodynamic instabilities within the shear layer interact continuously with the acoustic field in the side branch while being convected across the orifice. This interaction can be constructive or destructive, depending on the Strouhal number, and can be estimated using the low Mach number approximation for the time-averaged power proposed by Howe [11]:

$$\langle P \rangle = -\rho_0 \int_V \langle (\boldsymbol{\omega} \times \mathbf{v}) \cdot \mathbf{u}' \rangle \, \mathrm{d}V, \tag{16}$$

where $\boldsymbol{\omega} = \nabla \times \mathbf{v}$ is the vorticity vector, $\mathbf{v}$ is the total fluid velocity, $\mathbf{u}'$ is the acoustic particle velocity, and V is the volume enclosing the vorticity. If the time-averaged power is positive, sound is generated. Conversely, sound energy is lost to the hydrodynamic field if the time-averaged power is negative. If the amplitude of the acoustic particle velocity relative to the mean flow velocity is sufficiently small (in the order of 10^{-3}), this process is linear [26,8] and the model proposed in Eq. (5) holds—that is, information about the flow–acoustic interaction is included in the linear scattering matrix obtained from an experiment. On the other hand, when the ratio of the acoustic particle velocity to the mean flow velocity is higher (in the order of 10^{-1}), the system may be nonlinear and the shear layer disturbances may tend to roll up into discrete vortices.

The hydrodynamic instabilities are convected downstream with a velocity U_c, resulting in a travel time from the separation edge to the downstream edge of $\tau = d/U_c$, where d is a characteristic length of the orifice. Comparing this travel time to the oscillation period, T, of the acoustic field, a type of mode number, $n = d/(U_c T)$, is obtained. For each mode number n, a Strouhal range where self-sustained oscillations are possible may be calculated [11,27]. As shown by Hofmans [15],

and discussed in Section 4, the actual configuration of the hydrodynamic and acoustic fields greatly influences the coupling between them. To calculate the time-averaged acoustic power using Eq. (16), a model for the vortex distribution is required. Using Bruggeman's model [26] for the vorticity, the following expression for the limit values of the Strouhal number where self-sustained oscillation may occur was derived by Meissner [27]:

$$St+\tan^{-1}\left(\frac{1}{St}\right)=2n\pi\pm\frac{\pi}{2}. \tag{17}$$

With the present methodology, the Strouhal regions where the system amplifies or attenuates the incoming acoustic disturbance can be found by forming a power balance over the three-port. The scattering matrix gives the relationships between the travelling wave amplitudes in the ports. Thus, assuming reflection-free terminations in the two ports not observed, the total relative power in the system when exciting from the third port is given by the sum of the acoustic power reflected at the excited port and the acoustic power transmitted into the other two ports. The acoustic power is given directly as the product of the fluctuating stagnation enthalpy and mass, but is here expressed in terms of the scattering matrix elements based on acoustic pressure with the appropriate compensation term:

$$\langle P^{\mathrm{I}}_{\mathrm{out}}\rangle/\langle P^{\mathrm{I}}_{\mathrm{in}}\rangle=\frac{|R_{\mathrm{I}}|^2(1-M_{\mathrm{I}})^2A_{\mathrm{I}}}{(1+M_{\mathrm{I}})^2A_{\mathrm{I}}}+\frac{|T_{\mathrm{I-II}}|^2(1+M_{\mathrm{II}})^2A_{\mathrm{II}}}{(1+M_{\mathrm{I}})^2A_{\mathrm{I}}}+\frac{|T_{\mathrm{I-III}}|^2(1\pm M_{\mathrm{III}})^2A_{\mathrm{III}}}{(1+M_{\mathrm{I}})^2A_{\mathrm{I}}}, \tag{18}$$

$$\langle P^{\mathrm{II}}_{\mathrm{out}}\rangle/\langle P^{\mathrm{II}}_{\mathrm{in}}\rangle=\frac{|R_{\mathrm{II}}|^2(1-M_{\mathrm{II}})^2A_{\mathrm{II}}}{(1-M_{\mathrm{II}})^2A_{\mathrm{II}}}+\frac{|T_{\mathrm{II-I}}|^2(1-M_{\mathrm{I}})^2A_{\mathrm{I}}}{(1-M_{\mathrm{II}})^2A_{\mathrm{II}}}+\frac{|T_{\mathrm{II-III}}|^2(1\pm M_{\mathrm{III}})^2A_{\mathrm{III}}}{(1-M_{\mathrm{II}})^2A_{\mathrm{II}}}, \tag{19}$$

$$\langle P^{\mathrm{III}}_{\mathrm{out}}\rangle/\langle P^{\mathrm{III}}_{\mathrm{in}}\rangle=\frac{|R_{\mathrm{III}}|^2(1\pm M_{\mathrm{III}})^2A_{\mathrm{III}}}{(1\pm M_{\mathrm{III}})^2A_{\mathrm{III}}}+\frac{|T_{\mathrm{III-I}}|^2(1-M_{\mathrm{I}})^2A_{\mathrm{I}}}{(1\pm M_{\mathrm{III}})^2A_{\mathrm{III}}}+\frac{|T_{\mathrm{III-II}}|^2(1+M_{\mathrm{II}})^2A_{\mathrm{II}}}{(1\pm M_{\mathrm{III}})^2A_{\mathrm{III}}}, \tag{20}$$

where A_i is the cross-sectional area of duct *i*, and the choice of sign in Branch III compensates for inflow or outflow. This approach is very similar to the integration of the acoustic power over the vorticity region described by Eq. (16). However, here the vorticity region is considered a black box with well defined ports in which the power can be determined. If there are no losses, the three contributions in each equation should add to unity, while with viscous wall losses only, their total should be close to unity. If the sum exceeds unity, more acoustic power is emitted from the system than is introduced, and hence power is transferred from the flow field to the acoustic field. If the three cases are added, one gets an estimate of the total power in the system; however, one should remember that the three cases are then considered uncorrelated.

Aurégan and Starobinski [28] suggested a similar approach which recently has been applied to predict whistling of confined orifice plates by Testud et al. [29]. Choosing state variables $\boldsymbol{a}$ and $\boldsymbol{b}$, related to each other by a scattering matrix $\mathbf{S}_p$ such that $\langle P_{\mathrm{inc}}\rangle=\mathbf{a}^*\mathbf{a}$ and $\langle P_{\mathrm{refl}}\rangle=\mathbf{b}^*\mathbf{b}$, the time-averaged acoustic power output is

$$\langle P_{\mathrm{out}}\rangle=\mathbf{b}^*\mathbf{b}-\mathbf{a}^*\mathbf{a}=\mathbf{a}^*(\mathbf{S}_p^*\mathbf{S}_p)\mathbf{a}-\mathbf{a}^*\mathbf{a}. \tag{21}$$

This equation is positive for a system that generates sound. Now, as before, normalize the incident acoustic power to unity—that is, set $\mathbf{a}^*\mathbf{a}=1$. Then the reflected acoustic power is given by the value of the first part of Eq. (21). This quadratic form is symmetric and positive definite, and thus it can be transformed into a diagonal form:

$$\mathbf{b}^*\mathbf{b}=\mathbf{a}^*(\mathbf{S}_P^*\mathbf{S}_P)\mathbf{a}=\sum_n\lambda_n|a'_n|^2, \tag{22}$$

where λ_n are the real and positive eigenvalues of $(\mathbf{S}_P^*\mathbf{S}_P)$ and the vector $\mathbf{a}'$ is given by $\mathbf{a}=\mathbf{T}\mathbf{a}'$. The transformation matrix $\mathbf{T}$ is a unitary matrix where the columns represent the eigenvectors of the Hermitian matrix $(\mathbf{S}_P^*\mathbf{S}_P)$. Finally, inserting Eq. (22) into Eq. (21), the maximum and minimum time-averaged acoustic power outputs are expressed as [28]

$$\langle P_{\mathrm{max}}\rangle=\lambda_{\mathrm{max}}-1, \tag{23}$$

$$\langle P_{\mathrm{min}}\rangle=\lambda_{\mathrm{min}}-1. \tag{24}$$

That is, an eigenvalue larger than unity indicates sound production. Note that these results include all possible excitations. The actual relative excitation yielding a maximum or a minimum can be found by examining the corresponding eigenvector.

Section 4 presents a comparison of the three methods for predicting whistling—the theoretical expression in Eq. (17) and the measured results using either Eqs. (18)–(20) or the eigenvalue approach.

3. Experimental procedure

Fig. 2 shows a schematic of the test rig, in which all branches are cylindrical steel ducts of the same diameter, $d=0.057$ m, and the same material thickness, 0.002 m. The geometry of the orifice edge has an influence [8,30,31]. Here, well-defined sharp edges that were easy to implement were used. The mean flow velocity profile approaching the orifice also influences the results [8]. It was assumed here that the approximately $60d$ duct length from the inlet to the side branch provided a fully developed turbulent velocity profile.

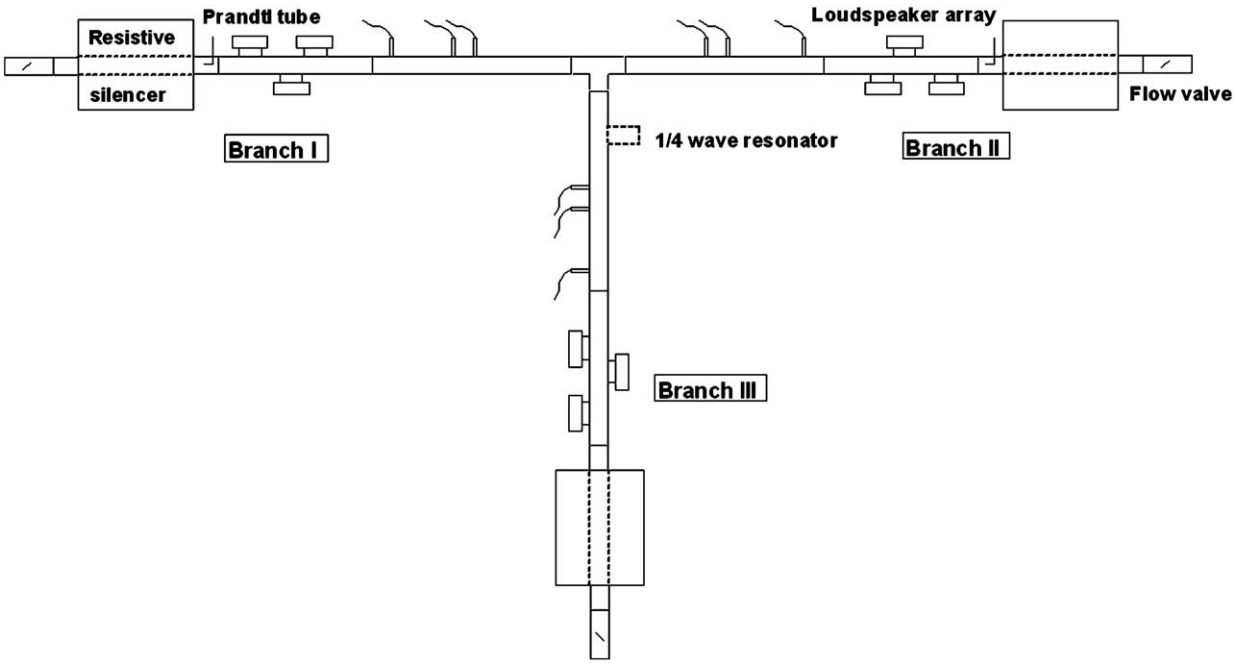

Fig. 2. Three-port test rig.

The quarter-wave resonator indicated in the sketch was only used for a restricted number of tests of the active properties of the system. For most of the tests, the quarter-wave resonator was not attached and Branch III was a straight duct like the two other branches. For the passive part of the measurements, it was preferred that no internal source be present. In particular, it was important that the system did not form a fluid-driven whistle, since that is a nonlinear phenomenon and the basis of the experimental procedure was to determine a linear aeroacoustic model. Hence, strong sound reflections were avoided and the excitation from the loudspeakers was kept to a moderate level. A study of the linearity of the system was performed and is presented in the results section.

The forward and backward travelling waves were determined by the two-microphone wave decomposition technique [32] using external sources [33]. The effect of uncorrelated disturbances, such as local turbulence, was minimized by using the transfer functions between the input voltage to the loudspeakers and the microphone signals, rather than using the microphone signals alone [34]. To cover the entire frequency range, two microphone separation distances were required, and therefore three microphones were used at each port. Sufficient excitation over the entire frequency range of interest was provided by an array of loudspeakers at each port. The separation distance between the loudspeakers in each array varied so as to avoid any wave interaction problems. The mean flow was provided by a pressurized anechoic stagnation chamber. The gas entered the test rig through either Branch I or Branch III, or through both simultaneously, thus permitting all combinations of the grazing–bias flow required. A flow leaving the main duct and entering the side branch is denoted bias outflow, while a flow entering the main duct from the side branch is denoted bias inflow. The actual relative mass flow in the ducts was regulated by valves at the ends of the ducts representing the ports. High performance resistive silencers were used at each port to reduce system reflections, thus minimizing the risk of whistling. The silencers also reduced flow noise generated by the flow regulating valves. The flow was monitored with Prandtl tubes in Branch I and Branch II. The gas temperature, T, was kept constant at approximately 20 °C during the experiments.

Bruel and Kjaer Type 4938 microphones and Nexus conditioning amplifiers were used with an HP VXI data acquisition system (an E1421B Mainframe with an E1432A data acquisition card). An E1432A source card was used to generate the excitation signal, which was then amplified with an NAD Model 319 stereo amplifier. For the passive data, swept sine excitation was used, with the number of averages taken continuously updated with respect to the signal to noise ratio. For the active data 4000 time samples were recorded. The frequency range was 50–2000 Hz, covering most of the plane-wave range. The digital frequency increment was 6.25 Hz.

4. Results

Initially a test with zero mean flow was performed. As discussed in the theory section, the position to which the three-port was reduced could now be determined. These results are also used to normalize the results with mean flow. That is,

results with mean flow are presented as the deviation from the zero mean flow case:

$$r_f = \mathrm{Re}(\overline{Z}) - \mathrm{Re}(\overline{Z}_{U=0}), \tag{25}$$

$$\chi_f = \mathrm{Im}(\overline{Z}) - \mathrm{Im}(\overline{Z}_{U=0}). \tag{26}$$

The difference in acoustic impedance with and without mean flow can be considered, under certain conditions, to be an indication of sound generation/attenuation [35]. In most previous work [8], the acoustic measurements were made in a duct with zero mean flow. This is in line with Lighthill's assumption of a stagnant uniform field between the source region and the observer. Here, mean flow is present in most of the configurations, making the interpretations less obvious. To confirm that sound is attenuated or dissipated one must apply the power balance procedure.

The Strouhal number, $St = fd_{\mathrm{eff}}/U_c$, shown in the presentation of results is based on the convection velocity of vorticity, U_c, across the orifice and the effective length of the orifice [26], $d_{\mathrm{eff}} = \pi d/4$. The actual correction factor, U_c/U_0, was chosen to give the best collapse of the data and is here 0.45. This agrees with results seen for other, similar, setups [26,36].

4.1. Acoustic impedance

The number of possible configurations of the mean flow and acoustic incidence is extensive; only a few illustrative examples were used in this study. Initially the results with zero mean flow are presented. Fig. 3 shows the influence on the reactance by the correction of the geometrical length of the side branch according to Eq. (6). For this case the actual end correction was 9.1 mm. Including the end correction, the reactance tends toward zero up to a Helmholtz number ($He = k_0 d$) of unity, after which it begins to deviate.

Fig. 4 shows the resistance and reactance for the three different impedance formulations in Eqs. (13)–(15). Note that with zero mean flow these formulations are identical to the ones obtained with the standard impedance formulation in terms of acoustic pressure over volume velocity. For the reactance, the results for the three formulations coincide well, indicating that the three-port is reduced to the correct position. The resistance tends toward the expected value in the low frequency limit but begins to deviate when the system can no longer be seen as acoustically compact ($He \ll 1$). With increasing Helmholtz number the system favours transmission from the side branch into the main duct rather than the opposite. Similar trends were observed by Parrondo et al. [37].

The linearity of the system was tested by varying the amplitude of the acoustic perturbation at a constant grazing mean flow Mach number. The grazing flow case was chosen for comparison with previous work by Kooijman et al. [8]. The response at the lowest excitation amplitude was chosen as the reference, and the results are presented as deviations from this reference case as the acoustic amplitude increases. Kooijman et al. [8] showed that the excitation level where the system becomes nonlinear varies with the characteristics of the system at a given frequency. In the interactive regions, with strong flow–acoustic coupling, the excitation level needed for the system to become nonlinear is lower than at points with low flow–acoustic interaction. Hence two different frequencies were tested, one corresponding to a Strouhal number of unity (150 Hz) and the other a higher frequency (600 Hz) where the flow–acoustic interaction is less pronounced. The results are presented in Fig. 5. At the excitation levels achievable with the present equipment, the response is linear at both frequencies tested. Up to the highest amplitude, where the ratio of the acoustic to mean flow velocity is in the order of 10^{-2}, the deviations are small and do not tend to grow. In the study by Kooijman, by comparison, nonlinear response was seen at a lower relative amplitude—in the order of 10^{-3} for the interactive flow–acoustic regions. Similar results as for the resistance were seen for the reactance, and also at other frequency points tested. In Fig. 6, the ratio of the acoustic to mean flow velocity is shown for the entire Strouhal number range used in later figures. Over the entire range, the ratio of the acoustic to mean flow velocity is within the linear range. For reference, the critical relative amplitudes proposed in the works by Bruggeman et al. [26] and Kooijman et al. [8] are shown.

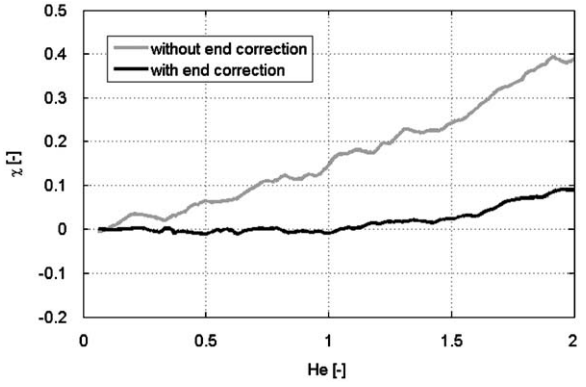

Fig. 3. Reactance with and without end correction according to Eq. (6).

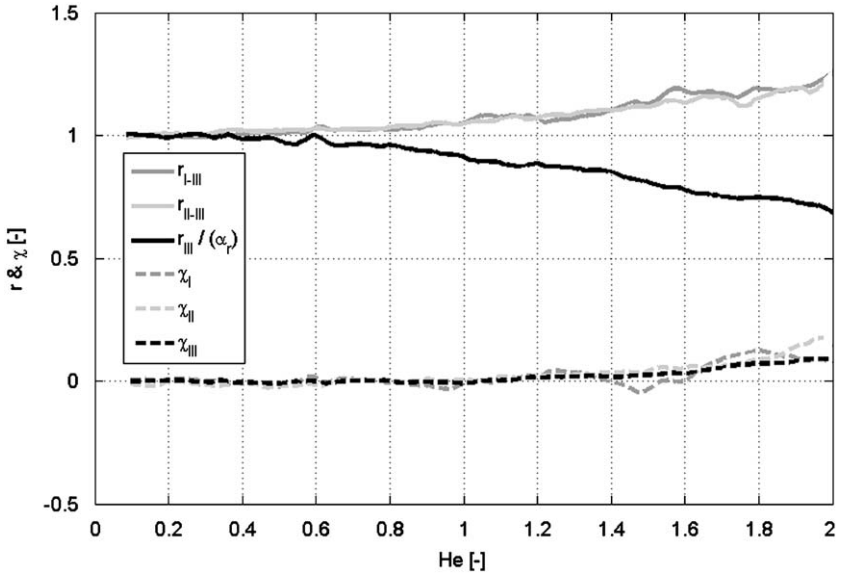

Fig. 4. Resistance and reactance for all three impedance formulations with no mean flow. α_r is the area ratio between the side branch and the main duct: $A_{III}/(A_I+A_{II})$.

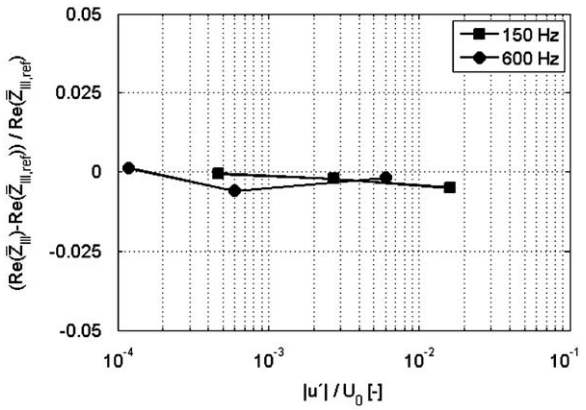

Fig. 5. Relative change of the resistance, $\mathrm{Re}(\overline{Z}_{III})$ when varying the amplitude of the acoustic perturbation at the orifice at a constant mean grazing Mach number of 0.05.

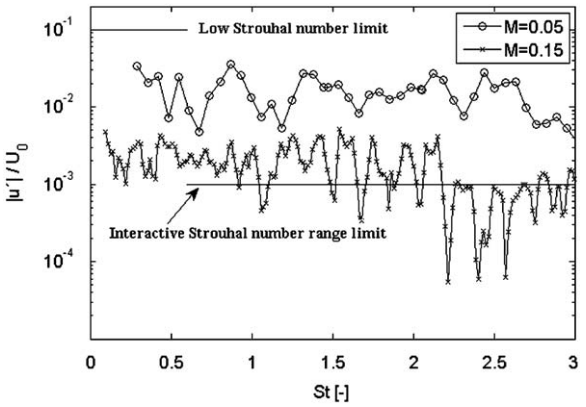

Fig. 6. Ratio of the acoustic to mean flow velocity at the orifice for typical test cases. The Mach number relates to grazing flow as presented in Fig. 7.

The influence of grazing flow alone on acoustic impedance is a well-researched area. However, most studies concentrate on orifices of small dimension compared to the main duct dimension. Here the relative orifice diameter is considerably greater, being equal to the diameter of the main duct. As will be shown, this has the advantage that a broader range of phenomena can be studied. Fig. 7 shows the orifice resistance normalized with the Mach number and the reactance normalized with the Helmholtz number for different grazing mean flow velocities. The normalization is chosen to stress the low Strouhal number behaviour. The data collapse well with Strouhal number. The Strouhal number ranges where the resistance is negative are centred at integer multiples of the Strouhal number, indicating flow–acoustic interaction. The change in sign of the reactance coincides with the extreme values of the resistance, as expected for a resonant system. Below the first hydrodynamic mode (approximately $St < 0.6$), both the normalized resistance and the normalized reactance tend toward the quasi-steady response. This response is usually interpreted as a pressure loss coefficient and end correction, respectively. Most previous work has focused on this range. With an orifice of smaller diameter than used here, the first hydrodynamic mode would be found at a correspondingly higher frequency.

The results in Fig. 7 are calculated using Eq. (15) – that is, the impedance seen from the side branch (Branch III). In Fig. 8 that formulation is compared to the results using the alternative formulations presented in Eqs. (13)–(14) – that is, the impedance with the incident acoustic wave coming from the up- and downstream ports and entering the side branch. The behaviour with excitation from the upstream port is similar to that seen previously: the oscillating behaviour of the resistance is maintained and is of a similar magnitude, and the reactance displays the same variations as before, but with a lower magnitude. More interestingly, the resistance and reactance seen from the downstream side differ significantly from that observed in the other two cases. The oscillating behaviour is not present, and the results do not deviate significantly from the zero mean flow case. A slight increase is seen in the reactance with increasing Strouhal number. Finally, the

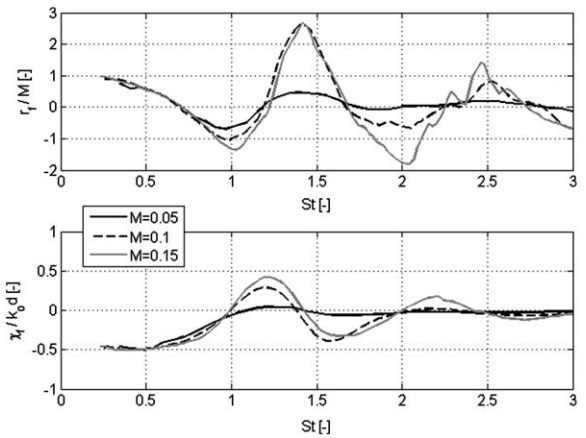

Fig. 7. Resistance and reactance with varying grazing mean flow Mach number, $\overline{Z}_{III}$.

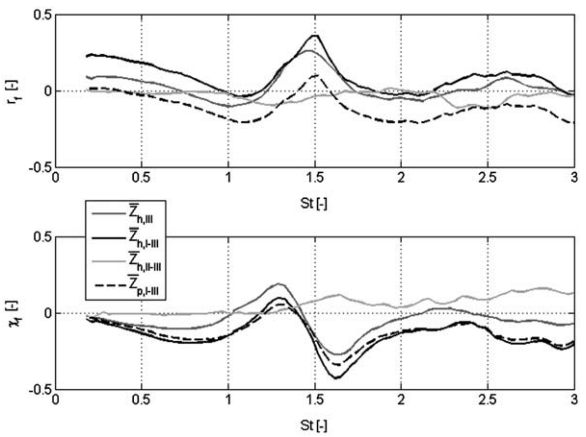

Fig. 8. Resistance and reactance as given by Eqs. (13)–(15) and with the impedance $\overline{Z}_{I-III}$ formulated also as p/q at $M=0.1$.

impedance $\overline{Z}_{p,\mathrm{I-III}}$ is plotted using the more common formulation of the acoustic pressure over volume velocity. The main characteristics are similar—the same scattering matrix elements are involved in the calculation—but there is a significant shift of the entire curve due to the omission of the compensation for mean flow. Given this last result, one would expect a large Strouhal number region where sound amplification could occur. It is clear that, depending on the choice of measurement method and impedance formulation, the estimated values for the acoustic impedance at a given frequency may differ significantly. This difference may explain some of the difficulties encountered when comparing previous authors' results.

As with grazing flow, the incidence of the acoustic waves influences the response of the orifice in the case of bias flow. Generally, the change with flow is less pronounced than with grazing flow; the resistance increases with the Mach number but the reactance is more or less unaffected except at small Strouhal numbers. In Fig. 9(a and b), the resistance for bias inflow and outflow, respectively, is seen at a bias Mach number of 0.05. For bias inflow, a region with negative resistance is centred around $St=0.5$ when the acoustic incidence is from Port I. However, forming a power balance according to Eq. (18) it is found that this indicates a redistribution of the relative power in the system, rather than a generation of sound. The response seen from the side branch ($\overline{Z}_{\mathrm{III}}$) is rather similar in the inflow and the outflow cases, but the response experienced from the upstream and downstream sides differs significantly. In Fig. 10 the reactance—expressed as an end correction—is given for the bias inflow case with the impedance seen from the side branch ($\overline{Z}_{\mathrm{III}}$). With a decreasing Strouhal number the relative end correction goes from the value with zero mean flow to a new level, where it stabilizes. This agrees with the results presented for an unconfined thick-walled (flanged) tube given by Peters et al. [38] and for a 90° sharp bend by Dequand et al. [39].

The influence of grazing–bias flow interaction on the acoustic impedance seen from the side branch, $\overline{Z}_{\mathrm{III}}$, is presented in Figs. 11 and 12. The results are for a grazing flow with a mean velocity corresponding to $M=0.1$ approaching the side branch. A partial stream was then either bled off to the side branch (outflow, Fig. 11) or introduced into the main duct from the side branch (inflow, Fig. 12). There is a substantial difference between the inflow and outflow cases. The outflow case is

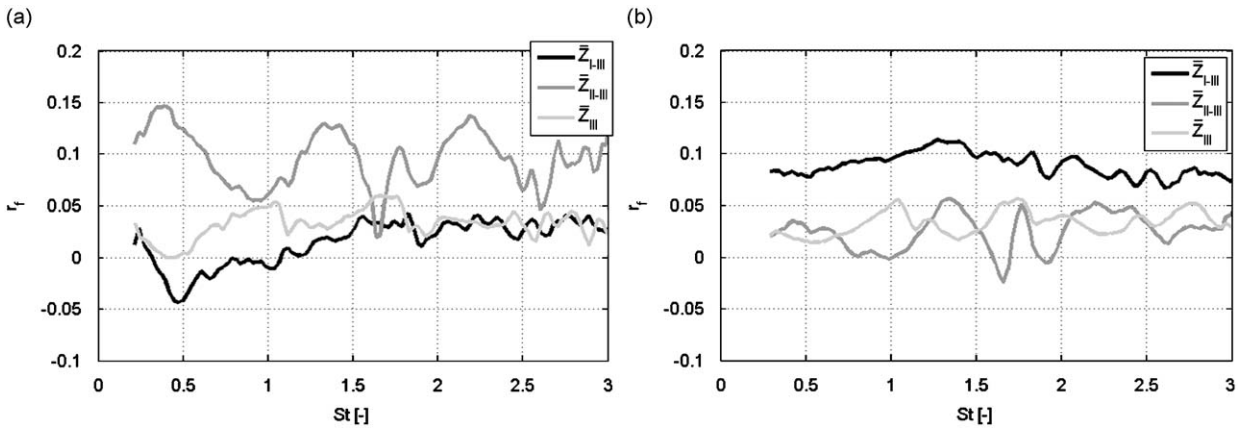

Fig. 9. Resistance with bias flow: (a) bias in $M=0.05$ and (b) bias out $M=0.05$. N.B. The Strouhal number is here defined as $St=fd/U$.

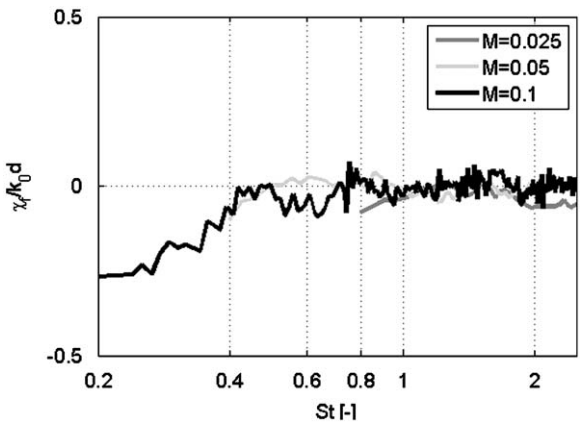

Fig. 10. End correction for bias in-flow and the impedance formulated according to Eq. (15). The Strouhal number is here defined as $St=fd/U$.

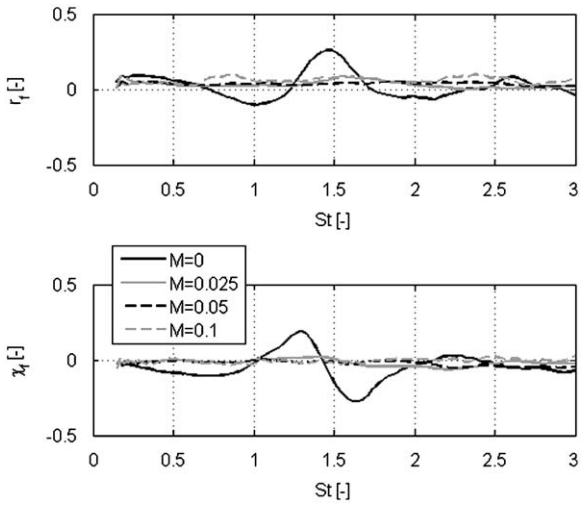

Fig. 11. Grazing–bias flow (out) interaction. M_G=0.1, varying bias mean flow velocity, $\overline{Z}_{III}$.

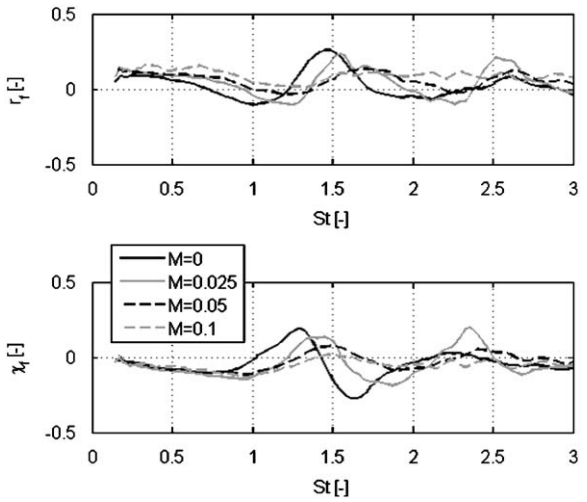

Fig. 12. Grazing–bias flow (in) interaction. M_G=0.1, varying bias mean flow velocity, $\overline{Z}_{III}$.

dominated by the behaviour seen for bias flow only. Even at the lowest bias Mach number, the oscillating behaviour produced by the grazing flow is completely cancelled. As for the bias outflow case, the resistance increases with increasing bias flow velocity, while the influence on the reactance is negligible.

In contrast, the grazing–bias inflow case shows a more interactive behaviour. With increasing bias flow velocity, the oscillating behaviour given by the grazing flow is gradually reduced but is still visible even at the highest bias flow rate. The peaks and troughs shift in Strouhal number with increasing bias inflow. The shift is significant initially but is less pronounced at higher flow rates. The Strouhal number used here is based on the convection velocity for grazing flow only and the effective diameter of the hole. Both the convection velocity and the effective length where the hydrodynamic and acoustic field can interact changes when adding bias flow and can contribute to the observed shift. A more detailed study of the flow field is required to explain this phenomenon.

4.2. Whistling potentiality

Regions where self-sustained oscillation can potentially be triggered in the system are shown in Fig. 13(a–c), where the three ports are studied individually. The total acoustic power out, as well as the acoustic power of the individual components, is calculated from the scattering matrix according to Eqs. (18)–(20). All results are for a test case with a

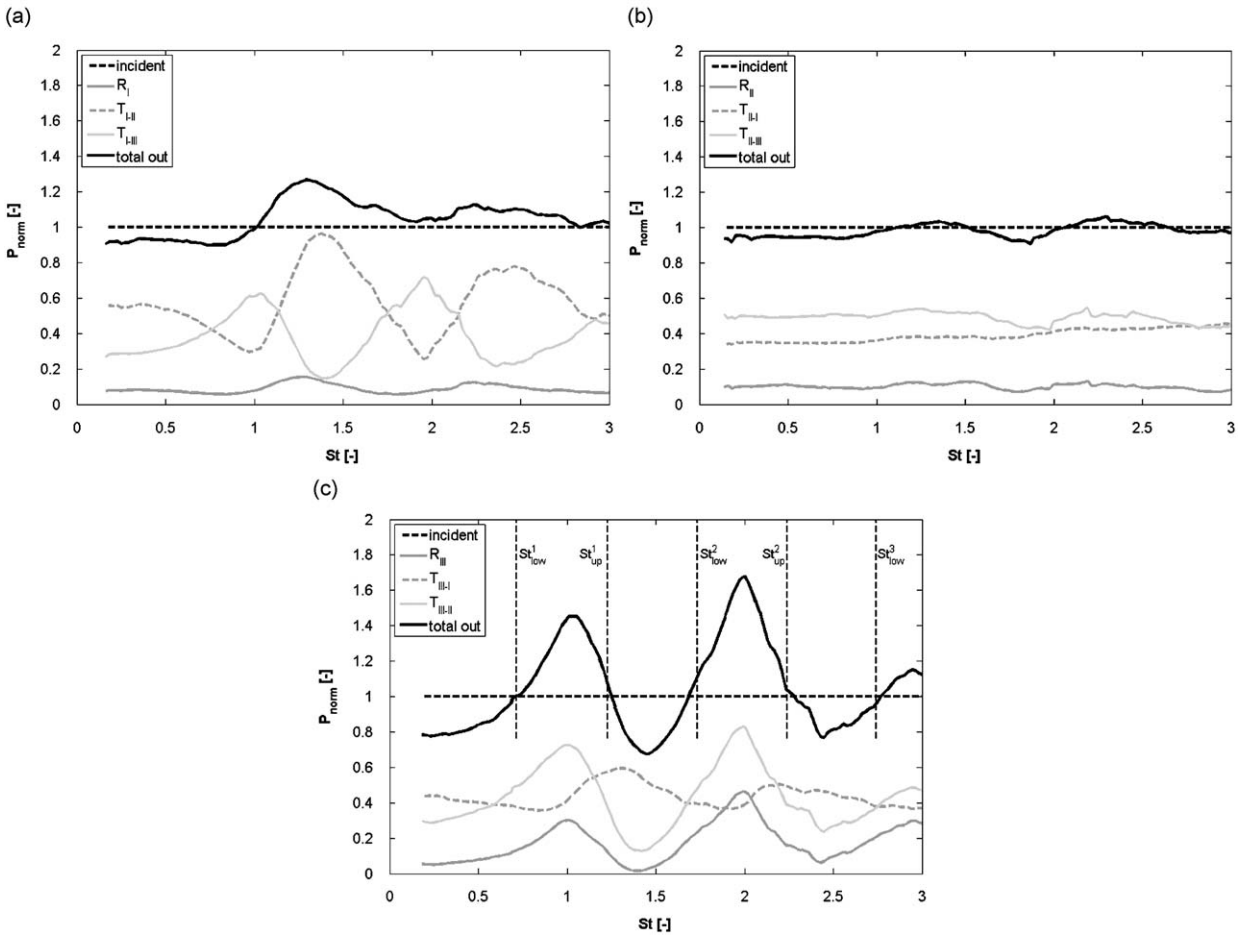

Fig. 13. Conservation of acoustic power over the three-port at $M_{grazing}$=0.15: (a) Port I, (b) Port II, and (c) Port III. The dashed vertical lines correspond to the upper and lower limits for the hydrodynamic modes predicted by Meissner [27].

grazing mean flow Mach number of 0.15. When exciting the three-port from Port III (Fig. 13c), the orifice is subjected to a uniform (plane-wave) time varying pressure. This is consistent with, for example, Meissner's [27] assumption. It is seen that distinct regions centred around integer multiples of the Strouhal number are formed where the system amplifies the incoming acoustic perturbation. This result is expected given the results for the resistance (see Fig. 7). The width of the regions agrees well with Meissner's results: the upper and lower Strouhal numbers for each mode predicted by Eq. (17) coincide with the experimental results. In studying the individual components, it is seen that the reflection and the transmission from the side branch to the downstream port are at maxima here. The transmission to the upstream port displays a maximum at a higher Strouhal number, approximately 1.3.

When the system is excited from Port I (Fig. 13a), a more interactive behaviour is observed. Again, the interaction with the side branch is seen at integer multiples of the Strouhal number. However, the maximum total acoustic power out is not observed in this region, but rather where the acoustic impedance of the side branch is high (St=1.2–1.3). The main contributor to this behaviour is an increased transmission to the downstream duct. This is information that is not obtained when studying only the acoustic impedance of the orifice. When the system is excited from Port II (Fig. 13b), the response is weaker. This was expected from the results for the resistance presented in Fig. 8. For this case, the acoustic field does not interact with the flow field as in the two other cases. Although the strong oscillating behaviour is lost, some response is seen at the same Strouhal number regions as in the Port I case.

The rather different results for the three ports are explained by the interaction of the grazing flow with the incident sound field. The modulation of the shear layer is triggered by the acoustic perturbation at the leading edge; this occurs in the Port I and Port III cases but not in the Port II case, where the incident travelling wave moves in the opposite direction of the flow and approaches the trailing edge. In the Port III case, the Strouhal numbers where the acoustic field interacts with the hydrodynamic instabilities coincide with the dominant contributions to the total power emitted. In the Port I case, the greatest contribution is at the Strouhal numbers where the side branch is blocked. Hofmans [15] studied a similar setup,

where the test object was a 2-D T-junction with a side branch of the same diameter as the main duct, and showed results for the grazing and bias (in and out) flow cases individually. For each flow case, the direction of incidence of the acoustic field also varied. As in this work, it was found that the shear layer was modulated by incident sound waves from both Ports I and III, and that the response differed between the cases. Unfortunately, there was no result for the Port II case for comparison.

Aurégan and Starobinski's [28] approach, Eqs. (23) and (24), is compared to the result for the total acoustical power emitted, arrived at by summation of Eqs. (18)–(20) and dividing by three, in Fig. 14. The eigenvalue approach yields the maximum and minimum values produced by any combination of excitations, while the summation of Eqs. (18)–(20) gives an approximation of the power from three uncorrelated cases. Hence, as expected, the summation of Eqs. (18)–(20) yields a value between the maximum and minimum, but it does predict the Strouhal number where flow–acoustic interaction occurs.

4.3. Whistling

One way to validate the three-port data is to change the acoustic load for a given flow case and then predict the acoustic response [21,22]. If the source data are correct and the T-junction can be represented as a linear time-invariant system, this should be a valid procedure. However, as discussed previously, conditions exist where the T-junction amplifies incoming sound waves to the point that the sound becomes nonlinear. To realize such a situation, a strong reflection is needed. This can be provided in Branch III, for instance, by adding a quarter-wave resonator. Such a resonator was designed and tuned against the second hydrodynamic mode—that is, for a Strouhal number of 2. For this setup, this corresponds to a frequency of approximately 1 kHz. The resonator setup is shown in Fig. 2, consisting of a quarter-wave resonator of length 0.085 m attached to Branch III at half-a-wavelength (0.17 m) into the duct from the orifice. The quarter-wave resonator is of the same diameter as the duct it is attached to—that is, $d=0.057$ m. At the resonance frequencies, where the input impedance of the resonator is small, a pressure minimum (velocity maximum) occurs at the resonator. Next, for maximum feedback effect (maximum velocity) in the vortex generation mechanism at the T-junction, the resonator is positioned at a multiple of half-a-wavelength into the side branch.

The source data were measured for this case and moved to the T-junction, this time taking the effect of the resonator in Branch III into account. If the modified system (the T-junction with a resonator at Branch III) is still a linear time-invariant system, the source data should be unchanged. Note that there is no flow in Branch III for the selected test case, and thus there is no sound generation from the resonator opening. The source data from the diagonal elements of the source cross-spectrum matrix, Eq. (4), with and without the resonator, are presented in Fig. 15. As the figure shows, the source data are almost identical except around a Strouhal number of two. The deviation means that in this Strouhal number region the three-port model is no longer valid. Thus, based on the previous discussion, the conclusion is that a fluid-driven whistle has

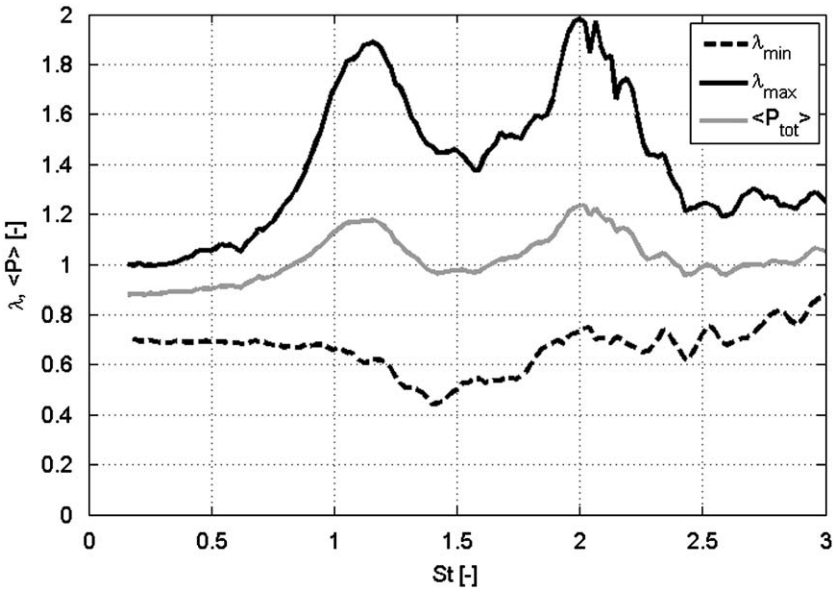

Fig. 14. Sound generation potentiality as identified by the power balance given by the sum of Eqs. (18)–(20) divided by three and the eigenvalue approach of Aurégan and Starobinski [28].

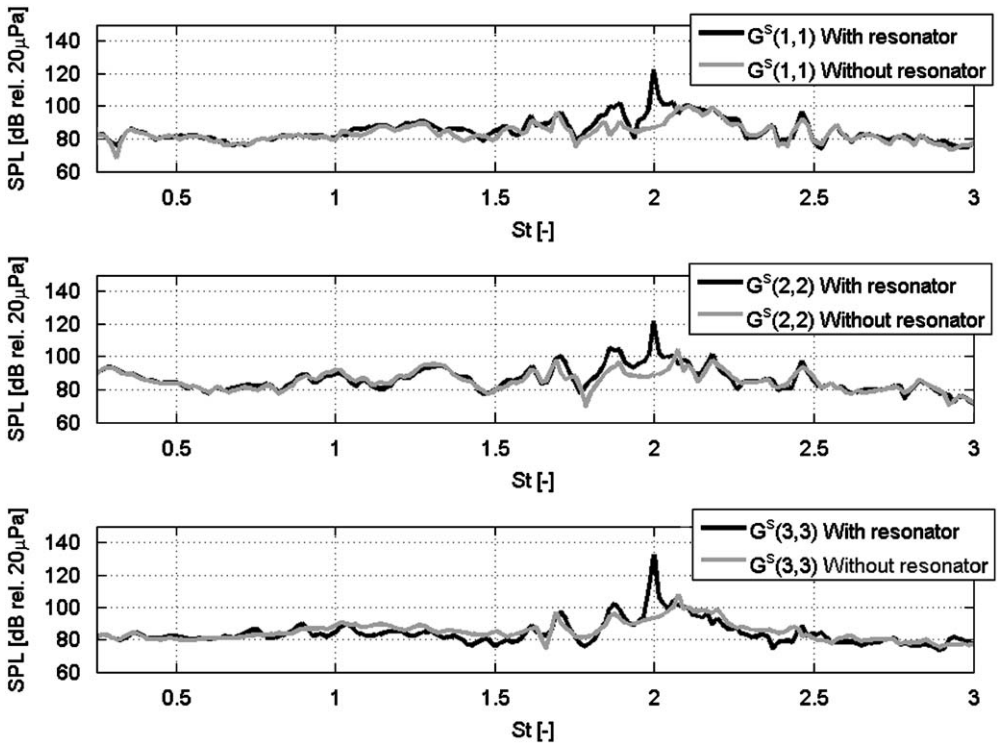

Fig. 15. Active results at each port with and without resonator at $M=0.15$.

been created. It is also apparent that in Branch III the resonator also produces a broadband effect—that is, it reduces the source strength by a few dB in a wide range around $St=2$.

5. Conclusions

A new method for making detailed investigations of the acoustic impedance of orifices is proposed. The method allows for any combination of grazing–bias flow. Also, the direction of incidence of the acoustic field may be varied. To the authors' knowledge, no other experimental study examines all the flow and acoustic field configurations studied in this work. The acoustic impedance was studied using a formulation based on the fluctuating stagnation enthalpy and mass, rather than the standard formulation involving the acoustic pressure and volume velocity. This study shows that the choice of measurement strategy, as well as the impedance formulation, greatly influences the results. This is one explanation for the large discrepancies in previous authors' results.

This study shows that, if the process is linear, information about source modulation (e.g., flow–acoustic interaction effects) is included in the scattering matrix obtained from the experiments. Thus passive data can be used to investigate the possible amplification of sound. By forming a power balance over the three-port system, the potential whistling regions are identified. The approach used in this work provides results in good agreement with the eigenvalue approach of Aurégan and Starobinski [28].

The acoustic impedance of the orifice varies significantly with different configurations of the hydrodynamic and acoustic fields. The interaction of the two fields is generally strongest when the acoustic field is incident from the side branch (Branch III) or from the upstream duct, while the response is much weaker with excitation from the downstream duct. With grazing flow, alternating Strouhal number regions of positive and negative resistance are found, and the positions of the maxima and the minima are dictated by the interaction of the acoustic and flow fields. The data collapse well using a Strouhal number based on the convection speed of vorticity across the orifice. Below the first hydrodynamic mode the response of the orifice can be estimated by a quasi-steady approach. The resistance is given by a coefficient times the Mach number, and the reactance is well described by a simple end correction. The effect of bias flow alone was studied for both inflow and outflow. In both cases, the influence on the reactance was negligible except for very low Strouhal numbers, and the resistance increased slightly with increasing Mach number. The grazing–bias flow interaction effect is different for the inflow and outflow cases. With grazing–bias inflow, the oscillating behaviour produced by the grazing flow is gradually reduced with increasing bias flow but is still present even at the highest bias flow rate. In the outflow case, the oscillating behaviour is lost, even at small bias flows, and the response is dictated by the bias flow. The results are

explained by the flow configurations: in the former case, the bias flow does not interfere with the leading edge, the one vital condition for triggering flow–acoustic coupling.

The T-junction is most prone to whistling when the acoustic field is incident from the side branch. The potential whistling regions are then clearly defined and correspond well with analytical models. If the system is excited from the upstream duct, a more interactive behaviour is observed. The maximum total power emitted from the three-port is then actually seen at the blocking Strouhal number, with the major contributor to this behaviour the increased transmission downstream. With excitation from the downstream side, the shear layer is not sufficiently triggered. The amplifying and blocking Strouhal number regions for the side branch are observable, but they are weak. To confirm that the system actually whistles at the identified regions, a resonator was designed. When the resonator was introduced, the linear three-port model broke down at the resonance frequency (as it should, as that model assumes a linear system), and a distinct tone radiated down the three ducts.

The method described in this study has proved stable and has produced results with excellent repeatability. The results provide a fundamental understanding of the phenomena involved, and the method is useful as an engineering tool for anyone involved in the design of flow-duct networks.

Acknowledgement

The financial support of the Swedish Energy Agency, Project 32022-1, is kindly acknowledged.

References

[1] D. Ronneberger, The acoustic impedance of holes in the wall of flow ducts, *Journal of Sound and Vibration* 24 (1972) 133–150.
[2] A.L. Goldman, R.L. Panton, Measurement of the acoustic impedance of an orifice under a turbulent boundary layer, *Journal of the Acoustical Society of America* 60 (1976) 1397–1404.
[3] J.W. Kooi, S.L. Sarin, An experimental study of the acoustic impedance of Helmholtz resonator arrays under a turbulent boundary layer, AIAA Paper 81-1998, 1981.
[4] A. Cummings, The effects of grazing turbulent pipe-flow on the impedance of an orifice, *Acustica* 61 (1986) 233–242.
[5] N.S. Dickey, A. Selamet, An experimental study of the impedance of perforated plates with grazing flow, *Journal of the Acoustical Society of America* 110 (2001) 2360–2370.
[6] X. Jing, X. Sun, J. Wu, K. Meng, Effect of grazing flow on the acoustic impedance of an orifice, *AIAA Journal* 39 (2001) 1478–1484.
[7] S.-H. Lee, J.-G. Ih, Empirical model of the acoustic impedance of a circular orifice in grazing mean flow, *Journal of the Acoustical Society of America* 114 (2003) 98–113.
[8] G. Kooijman, A. Hirschberg, J. Golliard, Acoustical response of orifices under grazing flow: effect of boundary layer profile and edge geometry, *Journal of Sound and Vibration* 315 (2008) 849–874.
[9] T. Elnady, Modelling and Characterization of Perforates in Lined Ducts and Mufflers, Ph.D. Thesis, Royal Institute of Technology, Stockholm, SE, 2004.
[10] X. Sun, X. Jing, H. Zhang, Y. Shi, Effect of grazing–bias flow interaction on acoustic impedance of perforated plates, *Journal of Sound and Vibration* 254 (2002) 557–573.
[11] M.S. Howe, *Acoustics of Fluid-Structure Interactions*, Cambridge University Press, Cambridge, 1998.
[12] K.S. Peat, J.-G. Ih, S.-H. Lee, The acoustic impedance of a circular orifice in grazing mean flow: comparison with theory, *Journal of Sound and Vibration* 114 (2003) 3076–3086.
[13] P.A. Nelson, N.A. Halliwell, P.E. Doak, Fluid dynamics of a flow excited resonance, part I: experiment, *Journal of Sound and Vibration* 78 (1981) 15–38.
[14] P.A. Nelson, N.A. Halliwell, P.E. Doak, Fluid dynamics of a flow excited resonance, Part II: flow acoustic interaction, *Journal of Sound and Vibration* 91 (1983) 375–402.
[15] G.C.J. Hofmans, Vortex Sound in Confined Flows, Ph.D. Thesis, Eindhoven University of Technology, Eindhoven, NL, 1998.
[16] P.D. Dean, An in situ method of wall acoustic impedance measurement in flow ducts, *Journal of Sound and Vibration* 34 (1974) 997–1030.
[17] D.L. Armstrong, F.R. Olsen, Impedance Measurements of Acoustic Duct Liners with Grazing Flow, *87th Meeting of the Acoustical Society of America*, New York, 1974.
[18] W.R. Watson, M.G. Jones, S.E. Tanner, T.L. Parrot, A finite element propagation model for extracting normal incidence impedance in non-progressive acoustic wave fields, NASA TM-110160, 1995.
[19] Y. Aurégan, M. Leroux, V. Pagneux, Measurement of liner impedance with flow by an inverse method, *10th AIAA/CEAS Aeroacoustic Conference*, Manchester, UK, 2004.
[20] T. Elnady, H. Bodén, An inverse analytical method for extracting liner impedance from pressure measurements, *10th AIAA/CEAS Aeroacoustic Conference*, Manchester, UK, 2004.
[21] H. Bodén, M. Åbom, Modelling of fluid machines as sources of sound in duct and pipe systems, *Acta Acustica* 3 (1995) 549–560.
[22] J. Lavrentjev, M. Åbom, Characterization of fluid machines as acoustic multi-port sources, *Journal of Sound and Vibration* 197 (1996) 1–16.
[23] C.J. Nederveen, J.K.M. Jansen, R.R.v. Hassel, Corrections for woodwind tone-hole calculations, *Acustica* 84 (1998) 957–966.
[24] V. Dubos, J. Kergomard, A. Khettabi, J.P. Dalmont, D.H. Keefe, C.J. Nederveen, Theory of sound propagation in a duct with a branched tube using modal decomposition, *Acta Acustica* 85 (1999) 153–169.
[25] C.L. Morfey, Acoustic energy in non-uniform flows, *Journal of Sound and Vibration* 14 (1971) 159–170.
[26] J.C. Bruggeman, A. Hirschberg, M.E.H. van Dongen, Self-sustained aero-acoustic pulsations in gas transport systems: experimental study of the influence of closed side branches, *Journal of Sound and Vibration* 150 (1991) 371–393.
[27] M. Meissner, Excitation of Helmholtz resonator by grazing air flow, *Journal of Sound and Vibration* 256 (2002) 382–388.
[28] Y. Aurégan, R. Starobinski, Determination of acoustical dissipation/production potentiality from the acoustical transfer function of a multiport, *Acta Acustica* 85 (1999) 788–792.
[29] P. Testud, Y. Aurégan, P. Moussou, A. Hirschberg, The whistling potentiality of an orifice in a confined flow using an energetic criterion, *Journal of Sound and Vibration* 325 (2009) 769–780.
[30] B.D. Knotts, A. Selamet, Suppression of flow–acoustic coupling in side branch ducts by interface modification, *Journal of Sound and Vibration* 265 (2003) 1025–1045.
[31] S. Dequand, X. Luo, J. Willems, A. Hirschberg, Helmholtz-like resonator self-sustained oscillations, part 1: acoustical measurements and analytical models, *AIAA Journal* 41 (2003) 408–415.
[32] A.F. Seybert, D.F. Ross, Experimental determination of acoustic properties using two-microphone random excitation technique, *Journal of the Acoustical Society of America* 61 (1977) 1362–1370.

[33] M.L. Munjal, A.G. Doige, Theory of a two source-location method for direct experimental evaluation of the four-pole parameters of an aeroacoustic element, *Journal of Sound and Vibration* 141 (1990) 323–333.
[34] M. Åbom, Measurement of the scattering-matrix of acoustical two-ports, *Mechanical Systems and Signal Processing* 5 (1991) 89–104.
[35] J.W. Coltman, Sounding mechanism of the flute and organ pipe, *Journal of the Acoustical Society of America* 44 (1968) 983–992.
[36] H.R. Graf, S. Ziada, Flow induced acoustic resonance in closed side branches: an experimental determination of the excitation source, *Symposium on Flow-Induced Vibration and Noise*, Vol. 7, ASME, 1992.
[37] J.L. Parrondo, J. Fernández, I. García, E. Ruiz, Noise transmission through duct divisions in air circuits, considered as three-port acoustic systems, *Journal of Sound and Vibration* 296 (2006) 183–194.
[38] M.C.A.M. Peters, A. Hirschberg, A.J. Reijnen, A.P.J. Wijnands, Damping and reflection coefficient measurements for an open pipe at low Mach and low Helmholtz numbers, *Journal of Fluid Mechanics* 256 (1993) 499–534.
[39] S. Dequand, S.J. Hulshoff, Y. Aurégan, J. Huijnen, R.T. Riet, L.J.V. Lier, A. Hirschberg, Acoustics of 90 degree sharp bends. Part II: low-frequency aeroacoustical response, *Acta Acustica* 90 (2004) 13–23.